Interaction of M^{3+} Lanthanide Cations with Diamide Ligands and Their Thia Analogues: A Quantum Mechanics Study of Monodentate vs Bidentate Binding, Counterion Effects, and Ligand Protonation

Christian Boehme, Bernard Coupez, and Georges Wipff*

Laboratoire MSM, UMR CNRS 7551, Institut de Chimie, 4, rue B. Pascal, 67 000 Strasbourg, France

Received: October 1, 2001; In Final Form: February 28, 2002

We report a quantum mechanical study on the interaction of M^{3+} cations (La^{3+}, Eu^{3+}, Yb^{3+}) with bidentate model ligands **L** of the malonamide type $\mathbf{L_{OO}}$ and their thia analogues $\mathbf{L_{OS}}$ and $\mathbf{L_{SS}}$**.** The chelate effect is analyzed, first by comparing the bidentate vs monodentate binding modes of the ligands in $MCl_3\mathbf{L}$ complexes, which indicates a surprisingly small preference for the former, and second, by an isodesmic reaction involving $MCl_3\mathbf{L}$ type complexes, which shows that two monodentate amide-like ligands bind better than one bidentate analogue, because of avoided strain induced upon metal binding. The role of counterions and stoichiometry is investigated by a comparison of the charged $M\mathbf{L}^{3+}$ complexes with the neutral $MCl_3\mathbf{L}$ and $MCl_3\mathbf{L}_2$ ones. In all systems, the order of ligand binding energies is $\mathbf{L_{OO}} > \mathbf{L_{OS}} > \mathbf{L_{SS}}$ for a given metal, following the order of calculated basicities. For a given ligand, the interaction energies increase in the order $La^{3+} < Eu^{3+} \leq Yb^{3+}$ in the $M\mathbf{L}^{3+}$ and $MCl_3\mathbf{L}$ complexes. With higher coordination numbers (bidentate $MCl_3\mathbf{L}_2$ complexes), the cation selectivity inverts to $La^{3+} > Eu^{3+} > Yb^{3+}$, as a result of "steric crowding" in the first coordination sphere, which penalizes binding to the smaller cations. The results are important in the context of modeling complexes of lanthanide and actinides, and for the design of selective ligands for metal separation.

1. Introduction

Understanding the factors that allow us to selectively bind trivalent lanthanide cations represents a challenging task from a basic point of view,[1] as well as for applications such as nuclear waste separation and minimization[2,3] or the design of photoactive systems.[4−7] Their behavior in condensed phases and in solution can be better understood when it is compared to the gas phase, i.e., in the absence of competition with polar solvent or other ligand molecules. Interesting insights into the energetics and structure of the complexes may be obtained from force field methods,[8−12] but the latter usually do not account for electronic effects (mostly polarization and charge transfer) as a function of the metal environment, or for changes in coordination patterns. This led us to undertake Quantum Mechanical (QM) computations to get information on structural, electronic, and energy features of noncovalent interactions between the cations and typical unidentate ligands such as $R_3P{=}O$,[13−15] $R_3P{=}S$,[16] amide, pyridine, triazine, or anisole derivatives.[17,18]

The present paper deals with an important class of malonamide type ligands and their thiocarbonyl analogues, interacting with lanthanide M^{3+} cations. Malonamides are important as an ecological (fully incinerable) alternative to the phosphorus containing CMPO (carbamoylphosphine oxide) ligands to extract M^{3+} ions from nuclear waste solutions ("DIAMEX" process),[2,19] and many derivatives have been developed.[20−22] Lanthanide complexes are also important as mimics of trivalent actinide complexes, which are less amenable to experimental investigations. According to recent X-ray spectrocopy studies in solution, Nd^{3+} and Am^{3+} malonamide complexes are both of $M(NO_3)_3$(malonamide)$_2$ type,[23] with strong similarities between the coordination spheres of both metal ions. Like CMPO or bidendate analogues,[24,25] malonamide moieties may also be grafted onto organized platforms such as calixarenes or resorcinarenes, likely leading to enhanced extraction properties. A number of X-ray structures of lanthanide complexes of malonamides have been reported, where the ligands generally bind in a bidentate fashion.[23,26−31] In the presence of coordinating anions, like NO_3^-, the maximum number of malonamides per metal is 2, while with noncoordinating anions, like PF_6^-, up to five ligands can bind to the largest ion La^{3+}.[26,32] Generally speaking, the polydentate chelate effect has been recognized as an important source of complex stabilization,[33−35] and a direct energy comparison of monodentate vs bidentate binding modes of a given ligand, not available from experiment, is an important issue of our study. Another issue concerns the comparison of oxygen vs sulfur binding sites, as sulfur compounds also complex lanthanide ions[36,37] and are considered, in the HSAB framework, as softer bases than oxygen analogues,[8,38,39] possibly leading to some lanthanide/actinide discrimination. Among the lanthanide series, they should also prefer the "softer" elements, e.g., La^{3+} over Yb^{3+}.

As ligands (noted **L**), we thus compare *N*,*N*,*N*′,*N*′-tetramethylmalonamide (noted $\mathbf{L_{OO}}$) and its thia-analogues, noted $\mathbf{L_{OS}}$ and $\mathbf{L_{SS}}$ (Figure 1). They interact with three lanthanide cations of decreasing size and incresing hardness: La^{3+}, Eu^{3+}, and Yb^{3+}. We first calculate the proton affinities of the ligands, as it is generally believed that the proton basicities correlate with cation basicities. We next study the intrinsic interaction energies ΔE between **L** and M^{3+} in the absence of other competing species in the charged $M\mathbf{L}^{3+}$ complexes. The effect of counterions is then investigated in the neutral $MCl_3\mathbf{L}$ complexes of 1:1 stoichiometry. Moving to higher stoichiometry in the $MCl_3\mathbf{L}_2$ complexes gives further insights into the effect of cumulative ligands in the coordination sphere of M^{3+}. For the three types

* Corresponding author. E-mail: wipff@chimie.u-strasbg.fr.

10.1021/jp0136617 CCC: $22.00
Published on Web 06/17/2002

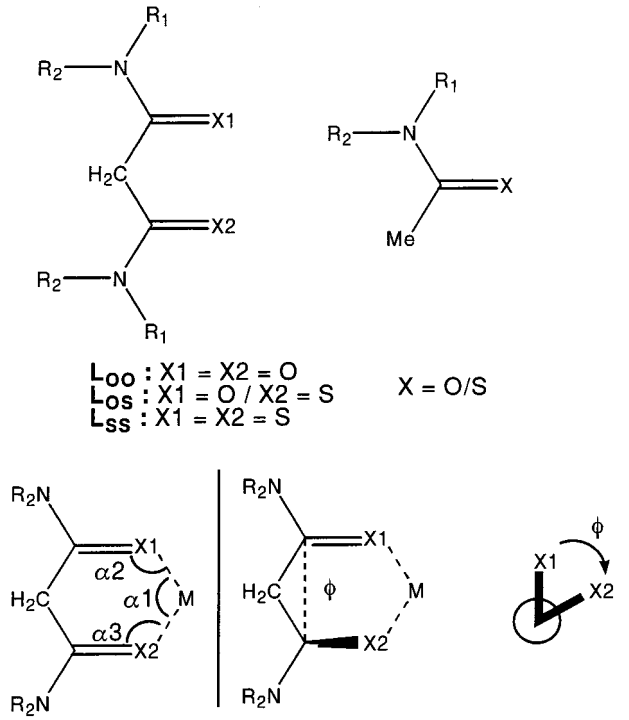

Figure 1. Simulated ligands and definitions of angles. ($R_1 = R_2 =$ Me).

of complexes, we focus on the interaction energies ΔE between **L** and the other part of the system. Structural features of the complexes are also described, as they reveal the stereochemical requirements for ion binding. It will be shown that they are markedly dependent on the type of ligand **L**, as well as on the presence of the other coordinated species (counterions, other ligands). Finally, we analyze the "chelate effect" by comparing the monodentate vs bidentate MCl_3**L** complexes, as well as via isodesmic reactions involving the two types of ligands. The gas phase structures cannot be directly compared with the solid state structures of analogous complexes, especially when the counterions are absent (ML^{3+} complexes) or when the first coordination shell is not filled (MCl_3**L** complexes). Generally speaking, the nature and properties of the first shell depend on the medium and are not necessarily the same in the gas phase as in condensed phases. We, however, also report the calculated gas-phase structures of the $Yb(NO_3)_3$**L**H_2O and $Yb(NO_3)_3L_2$ complexes, of 1:1 and 1:2 stoichiometry, respectively, for which X-ray data with analogous malonamide ligands are available.[23,30]

2. Methods

All compounds were fully optimized by quantum mechanical calculations at the Hartree−Fock (HF) level of theory, using the Gaussian98 software.[40]

The MCl_3**L**, ML^{3+} and LH^+ complexes were verified as true minima on the potential hypersurface by the analytical calculation of their force constants. Total energies including the effects of electron correlation have been obtained by single point calculations of the HF-derived structures, using density functional theory (DFT) with the B3LYP hybrid functional, as well as with Møller−Plesset perturbation theory of the second order (MP2). Relative energies of ligand binding ΔE have been calculated as shown in Figure 2 and have been corrected for basis set superposition errors (BSSE) using the counterpoise correction method.[41] The BSSE corrected B3LYP values are used throughout the presentation of the results, unless otherwise stated.

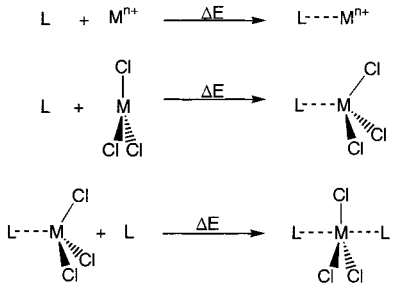

Figure 2. Definition of interaction energies ΔE.

As f-orbitals do not play a major role in metal−ligand bonds,[42,43] the 46 core and $4f^n$ electrons of the lanthanides are described by quasi-relativistic effective core potentials (ECP) of the Stuttgart group.[44,45] For the valence orbitals the affiliated (7s6p5d)/[5s4p3d] basis set was used, enhanced by an additional single f-function with an exponent optimized by Frenking et al.[46] The other atoms H, C, N, O, S, and Cl were described by the Dunning−Hay double ζ[47] plus polarization basis set D95(d), d-exponents being $\zeta_{3dC} = 0.75$, $\zeta_{3dN} = 0.80$, $\zeta_{3dO} = 0.85$, $\zeta_{3dS} = 0.532$ and $\zeta_{3dCl} = 0.60$.

The total DFT, HF, and MP2 energies of the systems are given in Table S1 and the BSSE corrected/uncorrected interactions energies are given in Table S2.

3. Results

We first discuss the ligand basicity toward proton and metal (LH^+ and ML^{3+} species). The effect of counterions is then considered in neutral MCl_3**L** complexes, for which bidentate and monodentate ligand binding modes are compared. Finally, moving to higher coordination numbers, we analyze MCl_3L_2 complexes.

The conformation of the ligands may be defined by the two H_2C-CX (X = O/S) dihedral angles. For simplicity, we use the ϕ angle between the two carbonyl dipoles (see Figure 1), which ranges from 0° for the cis ligand (planar binding) to 180° for the trans ligand and thus is a measure for the planarity of the bidentate binding mode of **L**. In the following, we focus on the questions of O/S binding sites, of counterions and stoichiometry, and of ligand binding mode. We refrain from describing all structures in detail. The coordinates of the optimized complexes with europium (intermediate between lanthanum and ytterbium) are given as supplementary information (Table S3) and a summary of the main structural parameters is given in Table 1 and Figures 4, 6, and 8.

3.1. Protonation Energies of the Diamide and Thia-Diamide Ligands. The optimized free ligands roughly adopt trans conformations, as a result of the dipole−dipole repulsions between the carbonyl groups. For $\mathbf{L_{OO}}$, $\mathbf{L_{OS}}$ and $\mathbf{L_{SS}}$ the dihedral angle ϕ is 162°, 135°, and 126°, respectively. This is somewhat larger than in solid-state structures of malonamides,[30] presumably because of substituent and packing effects. The $\mathbf{L_{OO}}$ and $\mathbf{L_{SS}}$ free ligands adopt a C_2 symmetry, as found for $\mathbf{L_{OO}}$ from other calculations at different computational levels.[48] Their main structural features are reported in Table 1.

Optimization of the protonated forms $\mathbf{L_{OO}H^+}$, $\mathbf{L_{OS}H^+}$, and $\mathbf{L_{SS}H^+}$ started from the trans conformations of the corresponding neutral forms but finally converged to cis structures ($\phi = 0°$), due to the formation of an internal "hydrogen bond" between the added proton and the unprotonated binding site (see Figures 3 and 4, and Table 1). The proton is bound asymmetrically between the two sites; i.e., one obtains one short covalent and one longer hydrogen bond, as observed in the X-ray structure of a protonated malonamide analogue (with R_1 = methyl, R_2,

TABLE 1: Selected HF/DZ* Optimized Distances (Å) and Angles (α1, α2, α3, φ, deg) of the Studied Compounds

	M−X1	M−X2	C1-X1	C2−X2	M−Cl	α1	α2	α3	φ
L_{OO}			1.210	1.210					162
L_{OS}			1.211	1.676					135
L_{SS}			1.677	1.677					126
HL_{OO}^{+}	0.989	1.579	1.276	1.221		145	110	106	0
HL_{OS}^{+} [a]	0.988	1.996	1.273	1.667		152	112	87	0
HL_{OS}^{+} [b]	1.338	1.779	1.211	1.727		142	113	96	0
HL_{SS}^{+}	1.352	2.103	1.721	1.669		152	95	92	0
LaL_{OO}^{3+}	2.191	2.191	1.299	1.299		74	143	143	0
EuL_{OO}^{3+}	2.092	2.092	1.304	1.304		77	142	142	0
YbL_{OO}^{3+}	2.004	2.004	1.308	1.308		81	140	140	0
LaL_{OS}^{3+}	2.189	2.729	1.301	1.773		78	152	110	23
EuL_{OS}^{3+}	2.087	2.626	1.305	1.779		82	150	108	24
YbL_{OS}^{3+}	1.997	2.536	1.308	1.785		86	149	106	25
LaL_{SS}^{3+}	2.717	2.744	1.774	1.768		82	110	118	57
EuL_{SS}^{3+}	2.613	2.639	1.780	1.773		86	108	115	60
YbL_{SS}^{3+}	2.524	2.550	1.787	1.779		91	105	111	62
$LaCl_3L_{OO}$	2.591	2.532	1.228	1.229	2.765	64	121	136	44
$EuCl_3L_{OO}$	2.455	2.418	1.229	1.227	2.660	66	122	138	37
$YbCl_3L_{OO}$	2.345	2.320	1.230	1.226	2.569	68	122	138	31
$LaCl_3L_{OS}$	2.525	3.235	1.228	1.708	2.740	67	149	91	68
$EuCl_3L_{OS}$	2.405	3.127	1.229	1.708	2.636	69	150	92	65
$YbCl_3L_{OS}$	2.287	3.057	1.228	1.706	2.545	71	153	92	60
$LaCl_3L_{SS}$	3.227	3.130	1.703	1.708	2.752	73	94	104	75
$EuCl_3L_{SS}$	3.174	3.003	1.702	1.710	2.649	75	94	104	75
$YbCl_3L_{SS}$	3.100	2.889	1.701	1.713	2.556	77	94	104	74
$LaCl_3L_{OO}$ mono	2.403		1.245	1.209	2.731		153		84
$EuCl_3L_{OO}$ mono	2.282		1.247	1.208	2.624		157		89
$YbCl_3L_{OO}$ mono	2.178		1.248	1.208	2.529		158		91
$LaCl_3L_{OS}$ mono[c]	2.478		1.237	1.696	2.701		136		69
$EuCl_3L_{OS}$ mono[c]	2.276		1.249	1.673	2.600		157		99
$YbCl_3L_{OS}$ mono[c]	2.173		1.250	1.673	2.507		156		101
$LaCl_3L_{SS}$ mono	3.009		1.742	1.672	2.689		100		113
$EuCl_3L_{SS}$ mono	2.887		1.745	1.673	2.589		100		113
$YbCl_3L_{SS}$ mono	2.780		1.748	1.673	2.498		100		113
$LaCl_3(L_{OO})_2$[d]	2.553	2.711	1.225	1.219	2.932	64	130	124	56
$EuCl_3(L_{OO})_2$[d]	2.435	2.612	1.224	1.218	2.827	65	132	124	54
$YbCl_3(L_{OO})_2$[d]	2.329	2.555	1.222	1.217	2.736	66	136	123	50
$LaCl_3(L_{OO})_2$[e]	2.619	2.648	1.225	1.223		63	124	128	57
$EuCl_3(L_{OO})_2$[e]	2.507	2.545	1.225	1.222		65	124	129	55
$YbCl_3(L_{OO})_2$[e]	2.409	2.457	1.224	1.221		67	125	130	52
$LaCl_3(L_{SS})_2$[d]	3.188	3.378	1.700	1.696	2.892	71	105	96	81
$EuCl_3(L_{SS})_2$[d]	3.077	3.338	1.701	1.693	2.773	72	105	96	80
$YbCl_3(L_{SS})_2$[d]	2.931	3.098	1.709	1.701	2.669	78	101	98	80
$LaCl_3(L_{SS})_2$[e]	3.305	3.434	1.699	1.692		69	96	102	82
$EuCl_3(L_{SS})_2$[e]	3.204	3.439	1.699	1.689		70	97	100	82
$YbCl_3(L_{SS})_2$[e]	2.948	5.793	1.716	1.669		44	68	107	83

[a] Protonation on the O atom. [b] Protonation on the S atom. [c] Coordination on the O atom. [d] Data of the first ligand. [e] Data of the second ligand.

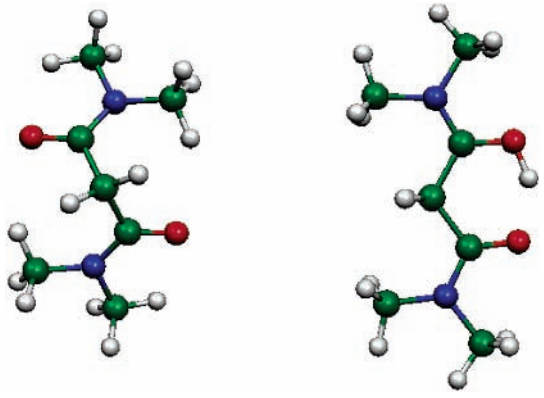

Figure 3. HF-optimized structures of L_{OO} (left) and $L_{OO}H^{+}$ (right).

cyclohexyl).[30] The S−H bond is longer than the O−H one (about 1.35 Å in L_{SS} and 0.99 Å in L_{OO}). The corresponding C=S−H and C=O−H angles (95° and 110°, respectively) are somewhat smaller than in the corresponding monofunctional analogues,[49] due to the formation of internal hydrogen bonds.

The basicities (see Table 2) follow the order $L_{OO} > L_{OS} > L_{SS}$. In L_{OS}, O-protonation is preferred over S-protonation (by 4.5 kcal mol^{-1}). This is an interesting result, as generally the proton affinity of sulfur is higher than that of oxygen in the gas phase,[50] and a previous work showed a higher proton affinity of thioamide compared to amide.[49] The difference in protonation energies between L_{OO} and L_{SS} is 9.3 kcal mol^{-1}, with total protonation energies of about 230 kcal mol^{-1}. This means that the basicities of the studied ligands are relatively close, and not markedly larger ($\Delta\Delta E$ is less than 10 kcal mol^{-1}) than those of the corresponding monoamide ligands.[49]

3.2. ML^{3+} Complexes: Intrinsic Properties of the M−L Bonds. The gas-phase binding between a lanthanide cation M^{3+} and a ligand **L** without counterions or additional ligands is determined solely by the intrinsic properties of the cation (size, hardness) and of the ligand (basicity, polarizability, hardness). Therefore, the theoretical investigation of the hypothetical ML^{3+} complexes allows one to judge the influence of these factors in the absence of other competing interactions. Sulfur is a larger and softer atom than oxygen, and the polarizability and softness

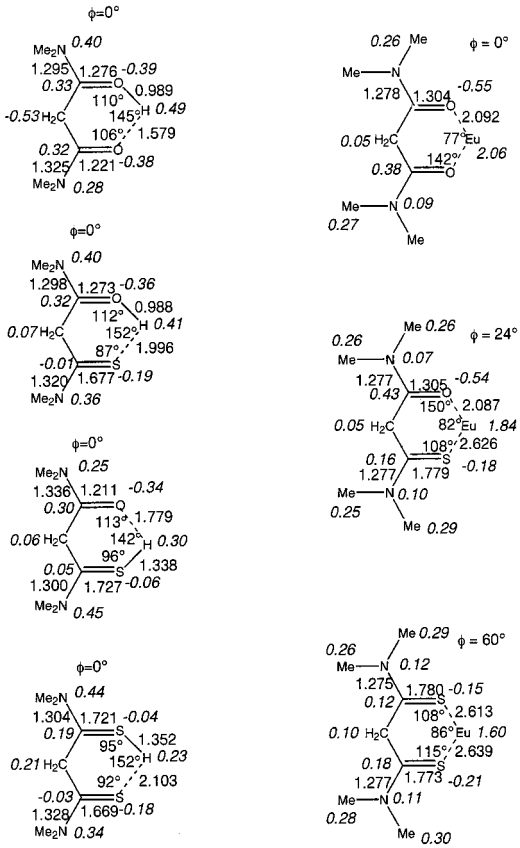

Figure 4. $\mathbf{LH}^+$ (left) and $\mathrm{M}\mathbf{L}^{3+}$ (right) complexes. $\mathbf{L} = \mathbf{L_{OO}}$, $\mathbf{L_{OS}}$, and $\mathbf{L_{SS}}$, from top to bottom. Schematic representation of the optimized structures, with selected distances (Å) and angles (deg). Mulliken charges in italics.

of the ligands follow the order $\mathbf{L_{OO}} < \mathbf{L_{OS}} < \mathbf{L_{SS}}$, which is the inverse of the proton basicities. Polarization effects should be largest for linear metal coordination to a given carbonyl group, as in monoamide M^{3+} complexes,[49] which is not compatible with bridging bidentate binding. In fact, the M−**L** interaction energies ΔE of the different ligands (see Table 2) follow their proton basicities, i.e., $\mathbf{L_{OO}} > \mathbf{L_{OS}} > \mathbf{L_{SS}}$, indicating that the higher polarizability of the sulfur binding sites is not sufficient to inverse the order of ΔEs. However, as reported for $R_3P{=}X$ type ligands,[16] this proton/metal basicity strength correlation is not a general rule. The total M−**L** interaction energies ΔE and their differences $\Delta\Delta E_M$ (i.e., differences between different **L** with the metal unchanged) are higher than the corresponding values for protonation of the ligands, due to the higher charge on the metal cation compared to a proton and the resulting larger charge-induced dipole interactions and charge transfers. The bigger induced polarization of $\mathbf{L_{OO}}$ and $\mathbf{L_{OS}}$ compared to the protonation is visible in the Mulliken charges (see Table 3), where the oxygen binding sites get more negative in the order free ligand < protonated ligand < $\mathrm{M}\mathbf{L}^{3+}$ complex (from about −0.3 to about −0.5 e^-). It should be noted, however, that in the case of the $\mathrm{M}\mathbf{L_{OS}}^{3+}$ and $\mathrm{M}\mathbf{L_{SS}}^{3+}$ complexes the sulfur binding sites are less negative than in the free ligands (by about 0.1 e^-). This is caused mainly by the charge transferred from sulfur to M, visible in the less positive M charges in the $\mathbf{L_{OS}}$ and $\mathbf{L_{SS}}$ complexes, compared to $\mathbf{L_{OO}}$ ones (1.84, 1.60, and 2.06 e, respectively, for europium).

Regarding the metal cation selectivity one notes that for all ligands the interaction energies ΔE with respect to M increase in the order $La^{3+} < Eu^{3+} < Yb^{3+}$, i.e., toward smaller size and increasing hardness. The differences $\Delta\Delta E_L$ in interaction energies of the same ligand with the different metal cations (or, in other words, the cation preferences for a given ligand) are about the same for all studied ligands ($\Delta\Delta E_L \sim 60$ kcal mol^{-1} from La^{3+} to Yb^{3+}).

In the $\mathrm{M}\mathbf{L_{OO}}^{3+}$ complexes (see Figures 4 and 5, and Table 1) the metal cation is bridging symmetrically over the two oxygen binding sites. Like $\mathbf{L_{OO}H}^+$, these complexes are planar, as one can see from the dihedral angle ϕ, which is 0°. The sulfur containing $\mathrm{M}\mathbf{L_{OS}}^{3+}$ and $\mathrm{M}\mathbf{L_{SS}}^{3+}$ complexes, on the other hand, are not planar (ϕ is about 25° and 60°, respectively), and the metal is not equidistant from the two binding sites, not even with the symmetric $\mathbf{L_{SS}}$ ligand. The reason is probably to accommodate both the longer M−S bonds (∼2.6 Å with M = Eu) and the smaller M−S−C angles (∼110° with M = Eu), compared to the corresponding values for the oxygen binding sites (Eu−O: ∼2.1 Å, Eu−O−C: ∼150°). The bite angle at the metal increases from $\mathbf{L_{OO}}$ (O−Eu−O = 77°) to $\mathbf{L_{SS}}$ (S−Eu−S = 86°). Comparison with the corresponding monoamide complexes in the same conditions (i.e., in the gas phase and using the same computational approach),[49] where the cation interacts with one carbonyl only, shows that with bifunctional ligands the M−O and M−S distances are longer (by about 0.1 and 0.2 Å, respectively), indicating that the bridging cation displays weaker bonds with each carbonyl moiety. Polarization effects are less important with bidentate than with monodentate ligands, where the C=O−M and C=S−M angles are quasi-linear instead of bent.

3.3. $\mathrm{MCl_3}\mathbf{L}$ Complexes: Influence of Counterions. In condensed phases the first coordination sphere of the metal is saturated by other ligands, anions, or solvent molecules. They modulate the M−**L** interaction by decreasing the charge of the cation, and even more by decreasing the space in the first coordination shell of M, which is available for the binding sites of **L**. To simulate the effect of counterions, we have calculated neutralized complexes of the type $\mathrm{MCl_3}\mathbf{L}$. As the corresponding coordination number (CN = 5) is still low compared to typical lanthanide values (CN = 7−10), the effects of steric crowding in the first coordination shell are presumably small.

In the $\mathrm{MCl_3}\mathbf{L}$ complexes the ligand **L** formally interacts with an MCl_3 moiety, leading therefore to reduced interactions, compared to the $\mathrm{M}\mathbf{L}^{3+}$ complexes. The optimized structures (see Figures 6 and 7, and Table 1) show indeed a lengthening of the M−**L** bonds (by about 0.3 to 0.5 Å), compared to the corresponding $\mathrm{M}\mathbf{L}^{3+}$ complexes. The lowered cation charge (q(M) ranges from 0.8 to 1.1 e; see Table 3) leads to less charge-induced dipole interaction and less ligand−metal charge transfer, thus weakening the M−**L** interaction and lengthening the bonds. The greater M−**L** bond lengths engender further changes, like the reduction of the C−X−M angles, and the enlargement of the dihedral angle ϕ with all ligands. For the $\mathbf{L_{OO}}$ complexes this means that the binding is no longer planar, in contrast to the $\mathrm{M}\mathbf{L_{OO}}^{3+}$ complexes. The complexed $\mathbf{L_{OS}}$ and $\mathbf{L_{SS}}$ ligands are also more gauche in $\mathrm{MCl_3}\mathbf{L}$ than in $\mathrm{M}\mathbf{L}^{3+}$ complexes, indicating that the gauche arrangement observed in solid-state structures with malonamide ligands[23,26,27,29] where ϕ angles of up to 51° can be observed[30] not only results from intrinsic interactions of the carbonyl groups with the metal but also depends on the amide substituents, as well as on interactions with other ligands and counterions. None of the complexes adopts a perfect 2-fold symmetry, partly due to the counterions. The two O−M distances with $\mathbf{L_{OO}}$, and the two S−M distances with $\mathbf{L_{SS}}$ differ, indicating that the two sites do not equally interact with the metal. Their difference is largest with La^{3+} (about 0.06 Å for the $\mathbf{L_{OO}}$ complex) and smallest with Yb^{3+}.

TABLE 2: B3LYP//HF, HF, and MP2//HF Calculated Ligand Binding Energies ΔE (kcal mol^{-1}), and Relative Interaction Energies $\Delta\Delta E$ (kcal mol^{-1}) of the Studied Compounds (Definitions in Figure 2)[a]

	DFT/DZ*//HF/DZ			HF/DZ*//HF/DZ*			MP2/DZ*//HF/DZ*		
	ΔE	$\Delta\Delta E_L$	$\Delta\Delta E_M$	ΔE	$\Delta\Delta E_L$	$\Delta\Delta E_M$	ΔE	$\Delta\Delta E_L$	$\Delta\Delta E_M$
HL_{OO}^+	−235.7		0.0	−234.3		0.0	−226.7		0.0
HL_{OS}^+ [b]	−232.6		+3.1	−229.1		+5.2	−223.3		+3.4
HL_{OS}^+ [c]	−228.1		+7.6	−225.7		+8.6	−220.5		+6.2
HL_{SS}^+	−226.4		+9.3	−219.9		+14.4	−215.4		+11.3
LaL_{OO}^{3+}	−311.5	0.0	0.0	−280.4	0.0	0.0	−297.4	0.0	0.0
EuL_{OO}^{3+}	−344.2	−32.7	0.0	−309.8	−29.4	0.0	−327.7	−30.3	0.0
YbL_{OO}^{3+}	−374.2	−62.7	0.0	−338.9	−58.5	0.0	−357.6	−60.2	0.0
LaL_{OS}^{3+}	−302.3	0.0	+9.2	−270.1	0.0	+10.3	−286.4	0.0	+11.0
EuL_{OS}^{3+}	−334.9	−32.6	+9.3	−299.6	−29.5	+10.2	−317.6	−31.2	+10.1
YbL_{OS}^{3+}	−365.5	−63.2	+9.2	−329.3	−59.2	+9.6	−347.8	−61.4	+9.7
LaL_{SS}^{3+}	−293.5	0.0	+18.0	−260.2	0.0	+20.2	−275.4	0.0	+22.0
EuL_{SS}^{3+}	−325.1	−31.6	+19.1	−288.7	−28.5	+21.1	−306.1	−30.7	+21.6
YbL_{SS}^{3+}	−354.2	−60.7	+20.5	−317.5	−57.3	+21.4	−335.8	−60.4	+21.8
$LaCl_3L_{OO}$	−40.7	0.0	0.0	−46.2	0.0	0.0	−44.0	0.0	0.0
$EuCl_3L_{OO}$	−42.7	−2.0	0.0	−48.3	−2.1	0.0	−43.0	+1.0	0.0
$YbCl_3L_{OO}$	−44.6	−3.9	0.0	−49.7	−3.5	0.0	−46.5	−2.5	0.0
$LaCl_3L_{OS}$	−36.0	0.0	+4.7	−40.9	0.0	+5.3	−40.1	0.0	+3.9
$EuCl_3L_{OS}$	−37.6	−1.6	+5.1	−42.3	−1.4	+6.0	−38.7	+1.5	+4.3
$YbCl_3L_{OS}$	−38.0	−2.0	+6.6	−42.3	−1.4	+7.4	−41.3	−1.2	+5.2
$LaCl_3L_{SS}$	−31.0	0.0	+9.7	−34.3	0.0	+11.9	−35.8	0.0	+8.2
$EuCl_3L_{SS}$	−31.8	−0.8	+10.9	−34.9	−0.6	+13.4	−34.1	+1.7	+8.9
$YbCl_3L_{SS}$	−31.7	−0.7	+12.9	−34.1	+0.2	+15.6	−36.3	−0.5	+10.2
$LaCl_3L_{OO}$ mono	−36.1	0.0	0.0	−41.5	0.0	0.0	−39.1	0.0	0.0
$EuCl_3L_{OO}$ mono	−39.8	−3.7	0.0	−44.3	−2.8	0.0	−39.4	−0.3	0.0
$YbCl_3L_{OO}$ mono	−42.1	−6.0	0.0	−47.1	−5.6	0.0	−44.3	−5.2	0.0
$LaCl_3L_{OS}$ mono[d]	−37.1	0.0	−1.0	−41.7	0.0	−0.2	−42.2	0.0	−3.1
$EuCl_3L_{OS}$ mono[d]	−38.9	−1.8	0.9	−43.0	−1.3	1.3	−40.2	2.0	−0.8
$YbCl_3L_{OS}$ mono[d]	−42.0	−4.9	0.1	−45.4	−3.7	1.7	−45.2	−3.0	−0.9
$LaCl_3L_{SS}$ mono	−29.8	0.0	6.3	−29.6	0.0	11.9	−29.7	0.0	9.4
$EuCl_3L_{SS}$ mono	−29.9	−0.1	9.9	−32.2	−2.6	12.1	−29.5	0.2	9.9
$YbCl_3L_{SS}$ mono	−30.8	−1.0	11.3	−33.1	−3.5	14.0	−33.7	−4.0	10.6
$LaCl_3(L_{OO})_2$	−15.2	0.0	0.0	−24.6	0.0	0.0			
$EuCl_3(L_{OO})_2$	−13.6	+1.6	0.0	−20.7	3.9	0.0			
$YbCl_3(L_{OO})_2$	−10.4	+4.8	0.0	−16.4	8.2	0.0			
$LaCl_3(L_{SS})_2$	−5.0	0.0	+10.2	−9.8	0.0	14.8			
$EuCl_3(L_{SS})_2$	−1.8	+3.2	+11.8	−6.5	3.3	14.2			
$YbCl_3(L_{SS})_2$	−2.9	+2.1	+7.5	−6.8	3.0	9.6			
	$\Delta E'$ [e]	$\Delta\Delta E'_L$	$\Delta\Delta E'_M$	$\Delta E'$	$\Delta\Delta E'_L$	$\Delta\Delta E'_M$			
$LaCl_3(L_{OO})_2$	−34.1	0.0	0.0	−32.9	0.0	0.0			
$EuCl_3(L_{OO})_2$	−33.7	+0.4	0.0	−35.9	−3.0	0.0			
$YbCl_3(L_{OO})_2$	−32.2	+1.9	0.0	−32.8	+0.1	0.0			
$LaCl_3(L_{SS})_2$	−21.8	0.0	+12.3	−21.9	0.0	+11.0			
$EuCl_3(L_{SS})_2$	−20.8	+1.0	+12.9	−20.3	+1.6	+15.6			
$YbCl_3(L_{SS})_2$	−23.8	−2.0	+8.4	−18.6	+3.3	+14.2			

[a] $\Delta\Delta E_L$ is the difference in ΔE's for a given ligand, relative to the lanthanum complex. $\Delta\Delta E_M$ is the difference in ΔE's for a given metal, relative to L_{OO} complex. [b] Protonation on the O atom. [c] Protonation on the S atom. [d] Coordination on the O atom. [e] Average interaction energy per ligand defined by $2\Delta E' = E(MCl_3L_2) - E(MCl_3) - 2E(L)$. The corresponding differences are defined as for ΔE.

When compared to the distances in the corresponding complexes with monoamide ligands optimized in the gas phase,[49] the M−O and M−S distances are about 0.2−0.3 Å longer, again indicating that the bridging metal displays weaker interactions with each binding site. Also note that the C═O−M and C═S−M angles (about 120° and 94° for L_{OO} and L_{SS}, respectively) are smaller than with monoamide ligands (165° and 100°), due to the bridging position of the cation. The bite angle at the bridging metal is again larger for the larger sulfur than the oxygen ligands (77° with L_{OO} and 86° with L_{SS}), and these values are about 10° smaller than in the ML^{3+} complexes, in relation with the longer M−L distances.

The ligand binding energies (from 31.8 to 42.7 kcal mol^{-1} for M = Eu) are much smaller than in the ML^{3+} complexes (from 325.1 to 344.2 kcal mol^{-1}), as expected. The order of ligands with respect to their binding strength toward M still follows their basicities. The differences $\Delta\Delta E_M$ are not as large as in the charged 1:1 complexes, however. The Yb/La metal ion preference, expressed by $\Delta\Delta E_L$, is much lower in the neutral ($\Delta\Delta E_L$ ranges from −0.7 to −3.9 kcal mol^{-1}) than in the charged complexes (−60.7 to −62.7 kcal mol^{-1}), and it almost vanishes for the ligand L_{SS}. There are two reasons for this: (i) The preference for the smaller cations can be attributed to the fact that their polarizing and charge attracting effects are especially strong because the ligands get closer to the charge. As the charge on the cations is diminished (e.g., from 2.06 e$^-$ in EuL_{OO}^{3+} to 0.96 e$^-$ in $EuCl_3L_{OO}$) and the M−L bonds get longer this effect loses importance. (ii) The more ligands are placed in the first coordination shell of the cations the more ligand−ligand repulsion occurs. This effect penalizes smaller cations more than larger ones.

3.4. MCl_3L_2 Complexes: Steric Crowding May Invert the Metal Binding Selectivity and Lead to Monodentate Coordination. In this section, the effect of adding another bidentate ligand L to the MCl_3L complexes is considered, thus forming MCl_3L_2 with a coordination number CN increased from 5 to 7, i.e., with increased steric crowding in the first coordination sphere. The CN is still somewhat smaller than the CN typically

TABLE 3: B3LYP//HF Calculated Mulliken Charges of the Studied Compounds

	Q(M)	*q*(Cl)	*q*(X1)	*q*(X2)	*q*(C1)	*q*(C2)	Σ*q*(ligand(s))
$\mathbf{L_{OO}}$			−0.34	−0.34	0.28	0.28	0.00
$\mathbf{L_{OS}}$			−0.35	−0.28	0.31	0.04	0.00
$\mathbf{L_{SS}}$			−0.28	−0.28	0.08	0.08	0.00
$H\mathbf{L_{OO}}^{+}$	0.49		−0.39	−0.38	0.33	0.32	0.51
$H\mathbf{L_{OS}}^{+}$ [a]	0.41		−0.36	−0.19	0.32	−0.01	0.59
$H\mathbf{L_{OS}}^{+}$ [b]	0.30		−0.34	−0.06	0.30	0.05	0.70
$H\mathbf{L_{SS}}^{+}$	0.23		−0.04	−0.18	0.19	−0.03	0.77
$La\mathbf{L_{OO}}^{3+}$	2.13		−0.56	−0.56	0.38	0.38	0.87
$Eu\mathbf{L_{OO}}^{3+}$	2.06		−0.55	−0.55	0.38	0.38	0.94
$Yb\mathbf{L_{OO}}^{3+}$	2.01		−0.54	−0.54	0.39	0.39	0.99
$La\mathbf{L_{OS}}^{3+}$	1.94		−0.55	−0.23	0.42	0.16	1.06
$Eu\mathbf{L_{OS}}^{3+}$	1.84		−0.54	−0.18	0.43	0.16	1.16
$Yb\mathbf{L_{OS}}^{3+}$	1.74		−0.53	−0.12	0.43	0.16	1.26
$La\mathbf{L_{SS}}^{3+}$	1.73		−0.20	−0.26	0.12	0.18	1.27
$Eu\mathbf{L_{SS}}^{3+}$	1.60		−0.15	−0.21	0.12	0.18	1.40
$Yb\mathbf{L_{SS}}^{3+}$	1.49		−0.10	−0.16	0.11	0.17	1.51
$LaCl_3\mathbf{L_{OO}}$	1.10	−0.49	−0.41	−0.42	0.38	0.39	0.31
$EuCl_3\mathbf{L_{OO}}$	0.96	−0.46	−0.40	−0.40	0.39	0.39	0.35
$YbCl_3\mathbf{L_{OO}}$	0.88	−0.46	−0.39	−0.39	0.39	0.39	0.41
$LaCl_3\mathbf{L_{OS}}$	1.04	−0.48	−0.41	−0.23	0.39	0.01	0.34
$EuCl_3\mathbf{L_{OS}}$	0.93	−0.46	−0.41	−0.22	0.40	0.01	0.37
$YbCl_3\mathbf{L_{OS}}$	0.86	−0.43	−0.38	−0.21	0.40	0.02	0.37
$LaCl_3\mathbf{L_{SS}}$	0.99	−0.49	−0.26	−0.24	0.09	0.06	0.38
$EuCl_3\mathbf{L_{SS}}$	0.87	−0.46	−0.23	−0.24	0.09	0.06	0.40
$YbCl_3\mathbf{L_{SS}}$	0.80	−0.44	−0.22	−0.23	0.09	0.06	0.42
$LaCl_3\mathbf{L_{OO}}$ mono	1.16	−0.48	−0.49	−0.33	0.39	0.34	0.22
$EuCl_3\mathbf{L_{OO}}$ mono	1.04	−0.46	−0.48	−0.33	0.39	0.33	0.26
$YbCl_3\mathbf{L_{OO}}$ mono	0.96	−0.43	−0.47	−0.33	0.39	0.33	0.26
$LaCl_3\mathbf{L_{OS}}$ mono[c]	1.08	−0.45	−0.44	−0.23	0.37	0.07	0.32
$EuCl_3\mathbf{L_{OS}}$ mono[c]	1.02	−0.42	−0.49	−0.22	0.41	0.05	0.25
$YbCl_3\mathbf{L_{OS}}$ mono[c]	0.95	−0.40	−0.47	−0.23	0.41	0.05	0.27
$LaCl_3\mathbf{L_{SS}}$ mono	1.04	−0.45	−0.31	−0.24	0.13	0.06	0.31
$EuCl_3\mathbf{L_{SS}}$ mono	0.90	−0.42	−0.30	−0.24	0.14	0.06	0.35
$YbCl_3\mathbf{L_{SS}}$ mono	0.83	−0.39	−0.29	−0.24	0.14	0.06	0.35
$LaCl_3(\mathbf{L_{OO}})_2$[d]	0.95	−0.55	−0.40	−0.37	0.37	0.41	0.31
$EuCl_3(\mathbf{L_{OO}})_2$[d]	0.82	−0.53	−0.38	−0.36	0.37	0.40	0.34
$YbCl_3(\mathbf{L_{OO}})_2$[d]	0.77	−0.53	−0.36	−0.34	0.38	0.40	0.35
$LaCl_3(\mathbf{L_{OO}})_2$[e]			−0.39	−0.37	0.39	0.34	0.27
$EuCl_3(\mathbf{L_{OO}})_2$[e]			−0.38	−0.37	0.40	0.35	0.32
$YbCl_3(\mathbf{L_{OO}})_2$[e]			−0.37	−0.36	0.41	0.36	0.34
$LaCl_3(\mathbf{L_{SS}})_2$[d]	0.82	−0.53	−0.23	−0.24	0.04	0.09	0.31
$EuCl_3(\mathbf{L_{SS}})_2$[d]	0.74	−0.51	−0.22	−0.23	0.04	0.09	0.27
$YbCl_3(\mathbf{L_{SS}})_2$[d]	0.72	−0.50	−0.24	−0.23	0.05	0.10	0.24
$LaCl_3(\mathbf{L_{SS}})_2$[e]			−0.23	−0.25	0.08	0.04	0.29
$EuCl_3(\mathbf{L_{SS}})_2$[e]			−0.23	−0.22	0.04	0.09	0.31
$YbCl_3(\mathbf{L_{SS}})_2$[e]			−0.26	−0.27	0.10	0.04	0.37

[a] Protonation on the O atom. [b] Protonation on the S atom. [c] Coordination on the O atom. [d] Data of the first ligand. [e] Data of the second ligand.

observed for lanthanides, but Cl^- is a rather large anion and thus should not support high CNs. Interestingly, although no constraint was imposed in the minimization process, the structure of the $MCl_3\mathbf{L}_2$ complexes looks very much like several experimental solid state structures of lanthanide nitrato complexes, where two bidentately coordinated oxygens would correspond to a chloride anion.[23,28,29] Schematically, the coordinated atoms form a distorted pentagonal bipyramid (see Figure 9), where four carbonyl groups and one anion sit in an equatorial plane, while two other anions are "axial", forming a Cl−M−Cl angle of about 160° with both $\mathbf{L_{OO}}$ and $\mathbf{L_{SS}}$ ligands. In the corresponding experimental structure, the equatorial anion is a "vertically oriented" nitrate. The two six-membered rings formed by the metal and the two ligands adopt a twisted boat conformation, more deformed with $\mathbf{L_{SS}}$ than with $\mathbf{L_{OO}}$ ligands, due to the smaller angles at sulfur.

In the $MCl_3\mathbf{L}_2$ complexes with both the $\mathbf{L_{OO}}$ and the $\mathbf{L_{SS}}$ ligands (see Figure 8 and Table 1) the two ligands are not bound equivalently to the cation. In the case of $\mathbf{L_{OO}}$ one ligand features

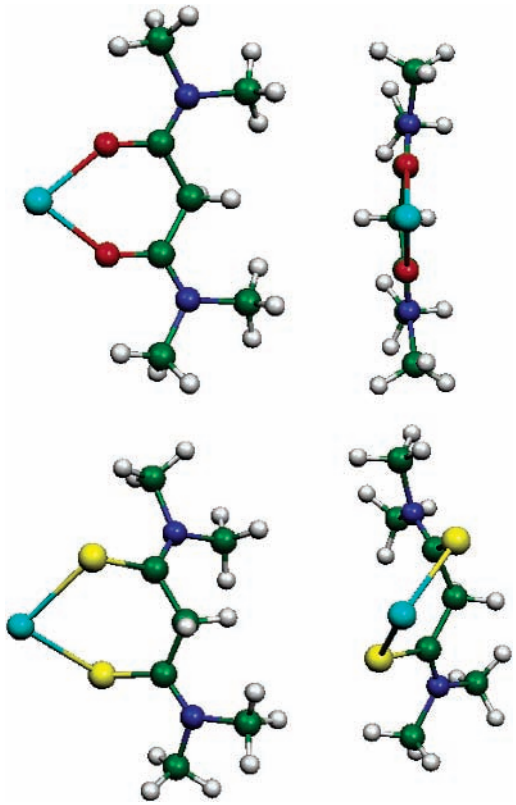

Figure 5. $M\mathbf{L}^{3+}$ complexes: optimized structures of the $Eu\mathbf{L_{OO}}^{3+}$ (top) and $Eu\mathbf{L_{SS}}^{3+}$ (bottom) complexes. Orthogonal views.

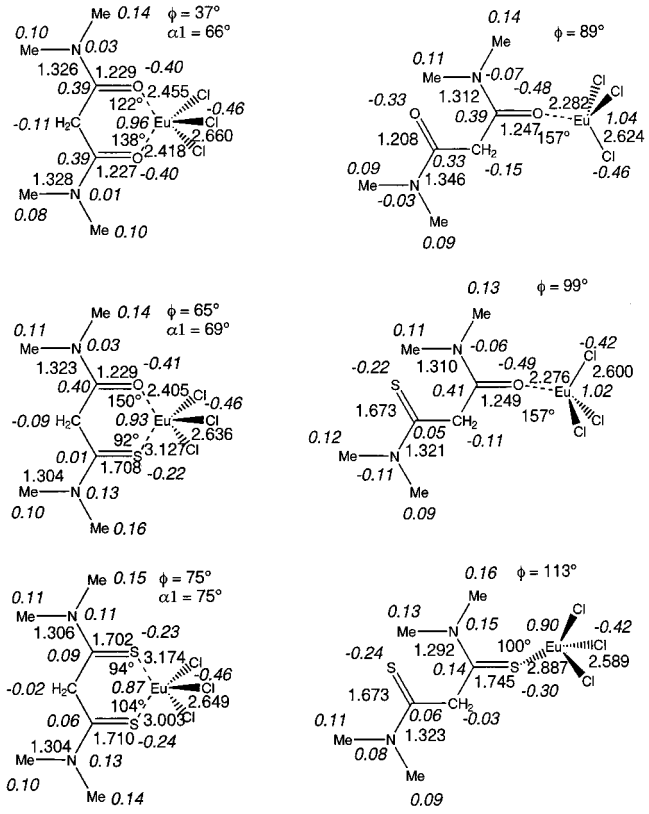

Figure 6. $MCl_3\mathbf{L}$ complexes with bidentate (left) and monodentate (right) bonding of **L**. $\mathbf{L} = \mathbf{L_{OO}}$, $\mathbf{L_{OS}}$ and $\mathbf{L_{SS}}$, from top to bottom. Schematic representation of the optimized structures, with selected distances (Å) and angles (deg). Mulliken charges in italics.

two quite different bond lengths (e.g., 2.435 and 2.612 Å with M = Eu; see Table 1 for M = La or Yb), while the other has

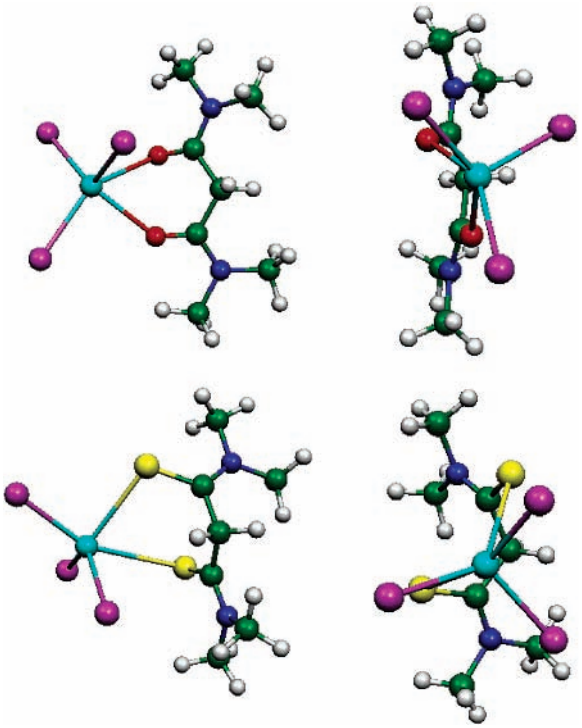

Figure 7. $MCl_3\mathbf{L}$ complexes: optimized structures of the $EuCl_3\mathbf{L}_{OO}$ (top) and $EuCl_3\mathbf{L}_{SS}$ (bottom) complexes with bidentate bonding of **L**. Orthogonal views.

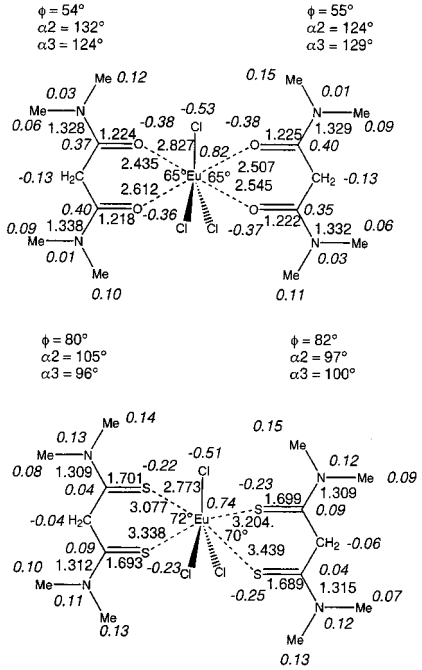

Figure 8. $EuCl_3(\mathbf{L}_{OO})_2$ (top) and $EuCl_3(\mathbf{L}_{SS})_2$ (bottom) complexes: schematic representation of the optimized structures, with selected distances (Å) and angles (deg). Mulliken charges in italics.

roughly equivalent bonds with lengths falling between those of the former (2.507 and 2.545 Å for Eu). In the case of $\mathbf{L}_{SS}$, both ligands have two different bond lengths, but one ligand is closer to the cation than the other. With few exceptions the bonds are longer than in the $MCl_3\mathbf{L}$ complexes. Also notice that the MCl_3 moiety moves from a pyramidal form in $MCl_3\mathbf{L}$ to a quasi-planar form in $MCl_3\mathbf{L}_2$ complexes, leading therefore to a zero dipole moment.

The interaction energies ΔE resulting from the addition of the second ligand **L** to $MCl_3\mathbf{L}$ (see Table 2) are only about

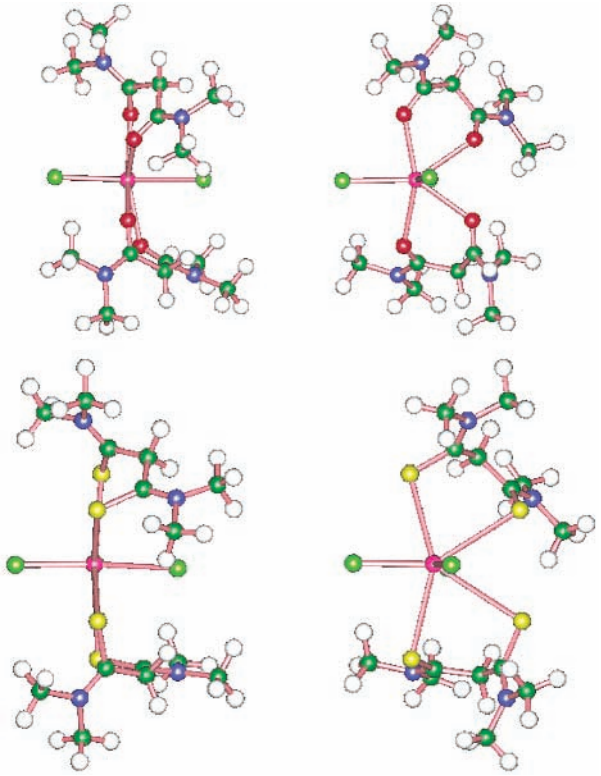

Figure 9. $MCl_3\mathbf{L}_2$ complexes: optimized structures of the $EuCl_3(\mathbf{L}_{OO})_2$ (top) and $EuCl_3\mathbf{L}_{SS}$ (bottom) complexes. Orthogonal views.

25% to 50% of those resulting from the addition of the first **L**, also showing the weakening of the M−**L** bonds visible in the M−**L** bond elongation. Two factors can be presumed to cause this. One is further diminishing of the M partial charge, leading to a lowered M−**L** attraction. However, the Mulliken charges of M (Table 3) in $MCl_3\mathbf{L}_2$ are only slightly lower than in $MCl_3\mathbf{L}$, so this can only be a minor influence. The other factor is the steric crowding of the first coordination sphere of M; i.e., it is related to the repulsive forces between the ligands and counterions. The forces include not only size effects (related to the dimensions of the ligands and van der Waals parameters as represented in molecular mechanics models)[8,9] but also electrostatic repulsions between negatively charged ligands or "parallel" dipoles. This factor is expected to gain importance with smaller cation size and larger binding sites, in agreement with our findings. Most notably the cation selectivity of the ligands $\mathbf{L}_{OO}$ and $\mathbf{L}_{SS}$, as expressed by $\Delta\Delta E_L$, is changed. $\mathbf{L}_{OO}$ now prefers the larger cations, and their order with respect to the interaction strength with $\mathbf{L}_{OO}$ becomes $La^{3+} > Eu^{3+} > Yb^{3+}$. The difference $\Delta\Delta E_L$ between La^{3+} and Yb^{3+} is 4.8 kcal mol^{-1}.

The situation is more complicated with the $\mathbf{L}_{SS}$ ligand: while La^{3+} is preferred by $\mathbf{L}_{SS}$ as well, its interaction energy is slightly lower with Yb^{3+} than with Eu^{3+}; i.e., the preference order is $La^{3+} > Yb^{3+} > Eu^{3+}$. The reason for this is found in the structure of $YbCl_3(\mathbf{L}_{SS})_2$ (Table 1), in which one of the $\mathbf{L}_{SS}$ ligands has become monodentate during the optimization process, thus alleviating the steric strain in the first coordination sphere of the cation.[51] Clearly, in the presence of relatively big chloride and sulfur binding sites, the limit has been reached when the $\mathbf{L}_{SS}$ ligands are bidentately coordinated to the smallest cation, despite the relatively low coordination number of 7.

The binding site size as a factor causing steric strain is also visible if one compares the ligand binding strength differences $\Delta\Delta E_M$ in $MCl_3\mathbf{L}_2$ to those in $MCl_3\mathbf{L}$ compounds. While $\mathbf{L}_{OO}$ is always bound more strongly than $\mathbf{L}_{SS}$ ($\Delta\Delta E_M$ is always

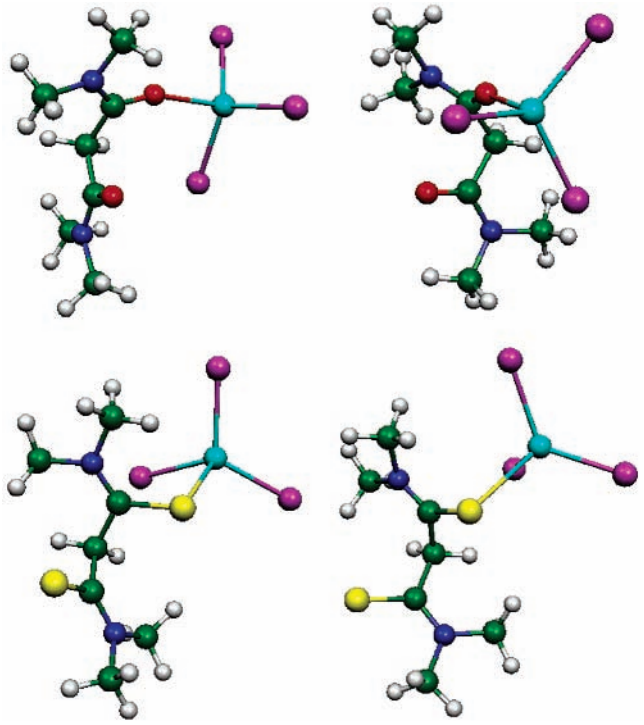

Figure 10. Optimized structures of the $EuCl_3\mathbf{L_{OO}}$ (top) and $EuCl_3\mathbf{L_{SS}}$ (bottom) complexes with monodentate bonding of **L**. Orthogonal views.

positive), the difference is larger ($\Delta\Delta E_M$ is higher) in the 2:1 compounds, due to the added steric strain effect (sulfur being bigger than oxygen atoms). $YbCl_3(\mathbf{L_{SS}})_2$ is an exception again, because of the monodentate binding mode of one $\mathbf{L_{SS}}$ ligand.

3.5. Diamides and Thia-Diamides as Monodentate Ligands in MCl_3L Complexes and a Comparison with Monoamides. In the above discussion of the complexes only the bidentate cis form of **L** was considered. However, to assess the strength of the bidentate preference, the bidentate forms of the $MCl_3\mathbf{L}$ complexes have to be compared with their monodentate analogues.

In these monodentate complexes, the ligand is not trans, but gauche (ϕ ranges from about 90° in $\mathbf{L_{OO}}$ to 120° in $\mathbf{L_{SS}}$; see Figures 6 and 10, and Table 1). The M−**L** bond distances for the binding site remaining complexed shorten considerably (by more than 0.1 Å), compared to the bidentate form, which indicates an enhanced interaction compensating for the lost second bond. The M−O and M−S distances with the coordinated carbonyl groups are nearly identical to those optimized in the corresponding monoamide complexes,[49] as are the C═O−M and C═S−M angles (about 160° and 100°, respectively), indicating the absence of constraints at the cation binding sites with both $\mathbf{L_{OO}}$ and $\mathbf{L_{SS}}$ ligands. Also note that the calculated C═O−M angles are in the range of experimental values for monamide ligands.[11]

The preference for the bidentate binding mode is found to be surprisingly small, about 2−3 kcal mol^{-1} for the symmetric $\mathbf{L_{OO}}$ and $\mathbf{L_{SS}}$ ligands. In the case of the asymmetric $\mathbf{L_{OS}}$ ligand, the monodentate mode (bound via the oxygen site) is even slightly preferred (by about 1 kcal mol^{-1} with lanthanum and europium), indicating that the enhancement of the M−O binding for this ligand and relief of internal ligand strain overcompensate the loss of the M−S bond. With the $\mathbf{L_{OO}}$ and $\mathbf{L_{SS}}$ ligands, the weak preference for bidentate coordination decreases from lanthanum to ytterbium (by 2.1−0.3 kcal/mol, respectively), in relation with the enhanced strain in the first coordination sphere when the cation size decreases.

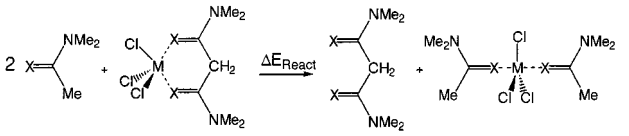

Figure 11. Isodesmic reaction used for the analysis of the chelate effect.

TABLE 4: B3LYP//HF, HF, and MP2//HF Calculated Reaction Energies ΔE_{React} in Kcal mol^{-1} (Definitions in Figure 11)

	DFT/DZ*/ HF/DZ*	HF/DZ*/ HF/DZ*	MP2/DZ*/ HF/DZ*
$LaCl_3\mathbf{L_{OO}}$	−22.7	−21.4	−22.9
$EuCl_3\mathbf{L_{OO}}$	−24.4	−22.6	−24.6
$YbCl_3\mathbf{L_{OO}}$	−25.1	−23.5	−25.8
$LaCl_3\mathbf{L_{SS}}$	−12.5	−14.7	−16.9
$EuCl_3\mathbf{L_{SS}}$	−12.9	−15.1	−17.3
$YbCl_3\mathbf{L_{SS}}$	−13.4	−15.4	−17.8

Another way to look at the problem of monodentate vs bidentate binding is to use the paradigm of the chelate effect as the basis for the analysis: a chelate ligand with a given number of binding sites possesses an intrinsic advantage over separate ligands, which together have the same number of binding sites.[33,34,56] The chelate effect is thus the positive free energy difference for the exchange of the chelate ligand with the separate ligands. In solution, this effect is generally attributed to entropic, rather than enthalpic factors, but the contribution of solvent and ligand itself is unclear. A discussion can be found in ref 33. To gain insights into the enthalpic component in the gas phase, we decided to calculate the ΔE_{react} energy for a model isodesmic reaction, in which a bidentate diamide ligand ($\mathbf{L_{OO}}$ or $\mathbf{L_{SS}}$) is replaced by two amide analogues, coordinated to a neutral MCl_3 moiety (Figure 11). In this model the coordination sphere of M is not saturated, allowing for a more widespread rearrangement of the coordinated species, therefore minimizing intrashell repulsions. According to our calculations on the bis-monoamide complex, this trans arrangement of the ligands is more stable than the cis isomer (by 5.7 kcal/mol with europium). The results of the isodesmic reaction (Table 4) show that for the two ligands and three cations studied, ΔE_{react} is negative; i.e., two monodentate ligands are clearly preferred (by 22.7−25.1 kcal mol^{-1} for $\mathbf{L_{OO}}$ and 12.5−13.4 kcal mol^{-1} for $\mathbf{L_{SS}}$). There are two main reasons for this. (i) As described above, the bidentate ligands cannot achieve optimal binding for both binding sites. The bidentate binding leads to the formation of a six-membered ring with the metal and ligand, and this may not be the most favorable ring size. A discussion can be found in ref 57. (ii) The coordination of bidentate amides requires a conformation that is above their energy minimum, with the two O−C dipoles parallel to each other. Due to polarization effects, which increase the carbonyle dipoles upon coordination to the metal, the dipole−dipole repulsions between the cis carbonyle groups are larger within the complex than within the uncomplexed ligands. According to the isodesmic reaction, the preference for two monodentate ligands increases toward smaller cations (by a few kcal mol^{-1} from La^{3+} to Yb^{3+}), where the aforementioned effect gets stronger.

3.6. Evaluation of the Theoretical Methods. Structural and Energy Data. The results presented so far are based on BSSE corrected DFT energies, calculated in the gas phase for HF optimized structures. In this paragraph it will be discussed if this choice of methods has a large influence on the results obtained, and how they compare to related solid state data. It has to be pointed out that exact energetic and structural data

TABLE 5: Selected HF-Optimized, DFT-Optimized, and X-ray Derived Distances (Å) and Angles (deg) of $Yb(NO_3)_3(H_2O)L$ and $Yb(NO_3)_3(L)_2$[a]

			M−X1	M−X2	M−NO_3	M−NO_3	M−NO_3	M−OH_2	α1	α2	α3	ϕ
						$Yb(NO_3)_3(H_2O)(\mathbf{L})$[30]						
X-ray structure	**L = L(Ph)**		2.296	2.274	2.836	2.883	2.867	2.350	76	131	136	14
HF/DZ*	**L = L_{OO}**		2.374	2.340	2.875	2.836	2.837	2.471	69	124	138	33
DFT/DZ*	**L = L_{OO}**		2.354	2.336	2.847	2.824	2.837	2.464	71	124	136	35
HF/DZ*	**L = L(Ph)**		2.379	2.346	2.870	2.836	2.839	2.482	70	124	136	40
						$Yb(NO_3)_3(\mathbf{L})_2$[23]						
X-ray structure	**L = L(Et)**	Lig1	2.292	2.280	3.295	2.894	2.840		71	141	137	23
HF/DZ*	**L = L_{OO}**	Lig1	2.391	2.373	3.391	2.871	2.864		68	139	133	40
DFT/DZ*	**L = L_{OO}**	Lig1	2.395	2.375	3.427	2.858	2.853		69	134	125	34
X-ray structure	**L = L(Et)**	Lig2	2.297	2.293					72	136	137	12
HF/DZ*	**L = L_{OO}**	Lig2	2.427	2.416					69	126	124	53
DFT/DZ*	**L = L_{OO}**	Lig2	2.355	2.376					71	128	127	52

[a] The X-ray structures of 1:1 and 1:2 complexes correspond to malonamide derivatives with R_1 = methyl and R_2 = phenyl **L(Ph)**,[30] $R_1 = R_2$ = ethyl[23] **L(Et)**, respectively (see definition in Figure 1). Ref 30: refcode: RIMQOT. Ref 23: refcode: WATZEN.

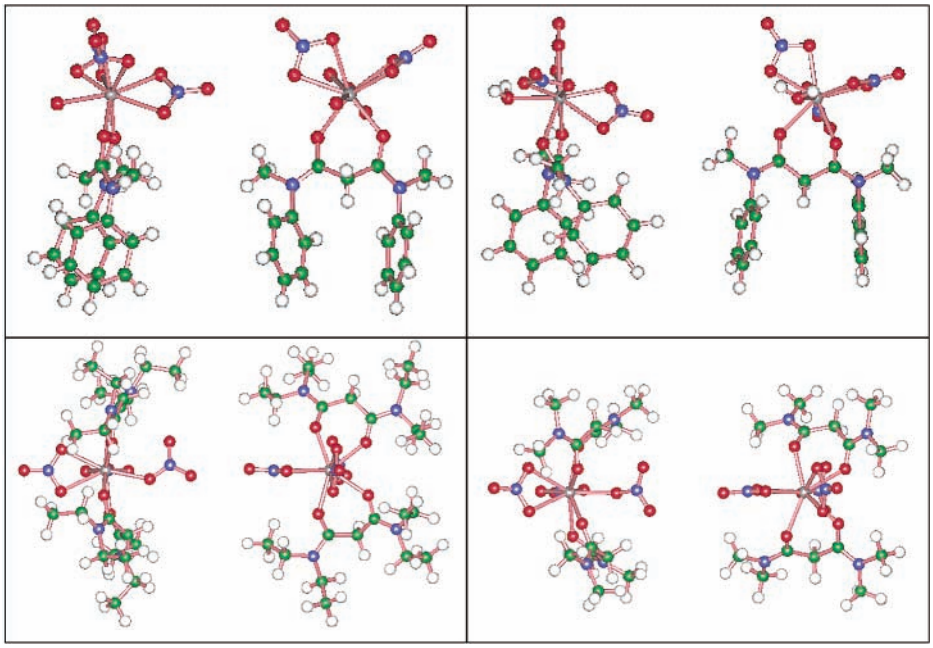

Figure 12. X-ray (left) and HF (right) optimized structures of $Yb(NO_3)_3(H_2O)$**L(Ph)** (top) and $Yb(NO_3)_3(\mathbf{L_{OO}})_2$ (bottom). Orthogonal views.

related to the systems this study focuses on are relatively sparse and deal with condensed phases only. All available X-ray structures with coordinated anions have bidentate nitrates instead of the chloride anions we used for simplicity. Therefore, we have conducted structure optimizations of two complexes, $Yb(NO_3)_3(H_2O)\mathbf{L_{OO}}$ and $Yb(NO_3)_3(\mathbf{L_{OO}})_2$, of which X-ray geometry data, albeit with differently substituted malonamide ligands, is available, to have examples for both 1:1 and 1:2 stoichiometry. In the experimental structure of the 1:1 complex, each amide moiety bears one phenyl instead of one methyl group, while in the 1:2 complex, it bears two ethyl groups. As this may somewhat modify the oxygen basicity[58] and ion binding strength, compared to the methyl substituents used in the calculations, we also optimized the "real" experimental $Yb(NO_3)_3(H_2O)$**L**(Ph) complex, where the **L**(Ph) ligands bears two phenyl groups trans to the carbonyl groups.

Computer graphics examination of the optimized structures shows that they retained their overall starting arrangements. Comparison of the X-ray data on $Yb(NO_3)_3(H_2O)$**L**(Ph) and the calculated structures with **L**(Ph) and $\mathbf{L_{OO}}$ ligands (see Table 5) reveals that the interactions between the metal and the negatively charged nitrate ligands are amplified in the gas phase, leading to some weakening of its interactions with the neutral ligands. As a result, the M−O_{NO_3} distances are on the average smaller in the calculated structures (0.03 Å between averages) than in the solid state. On the other hand, the M−$\mathbf{L_{OO}}$ and M−OH_2 bonds are longer (respectively by about 0.07 and 0.12 Å) in the theoretical structure. As the diamide $\mathbf{L_{OO}}$ ligand is less perturbed, the calculated C═O bonds are about 0.05 Å shorter. $\mathbf{L_{OO}}$ is also less planar in the calculated structure (ϕ = 33°) than in the X-ray structure (ϕ =14°). There is also some (minor) substituent effect at nitrogen, as the Yb−O distances are about 0.005 Å longer with the **L**(Ph) than with $\mathbf{L_{OO}}$, while the ligand is less planar (ϕ = 40°). For the 2:1 complex $Yb(NO_3)_3(\mathbf{L_{OO}})_2$ the X-ray vs calculated differences are somewhat larger than for the 1:1 complex, for example the average M−**L** distances differ by 0.11 Å. Overall the HF calculated structures agree sufficiently with the X-ray derived ones, especially if one considers that the former are "gas-phase" structures, while the latter are influenced by the crystal field and by neighbors in the crystal. Including an approximation for a solvent field has been shown to shorten M−**L** bonds by 0.05 Å.[59,60] The bite angle at the Yb center, as well as the C═O−Yb angles are within a few degrees identical in the calculated and experimental structures.

To assess the effects of electron correlation on the structures, the two ytterbium complexes with $\mathbf{L_{OO}}$ were also optimized on the DFT level of theory (see Table 5 and Figure 12). This

improves the agreement with the X-ray values, but in the case of $Yb(NO_3)_3(H_2O)\mathbf{L_{OO}}$ the changes are small (Table 5). For example, the difference between the average M−**L** distances drops from 0.07 to 0.06 Å. The improvement is more noticeable for $Yb(NO_3)_3(\mathbf{L_{OO}})_2$, where the M−**L** distances for the second ligand shorten by about 0.06 Å.

The energies used in this study all include electron correlation on the DFT level. If one compares these to the uncorrelated HF energies, one notes that applying DFT leads to an increase of the M−**L** interaction in the $M\mathbf{L}^{3+}$ complexes (by ∼30−40 kcal mol^{-1}), while it leads to a decrease in the $MCl_3\mathbf{L}$ complexes (by ∼2−6 kcal mol^{-1}). If one uses MP2 to include correlation effects, one obtains values between the HF and DFT results, except for the $MCl_3\mathbf{L_{SS}}$ complexes, where MP2 gives sometimes ΔE values higher than HF by 1−2 kcal mol^{-1}. All trends discussed are the same on both correlated and even on the uncorrelated HF level, excepting again the $MCl_3\mathbf{L_{SS}}$ complexes where MP2 gives slightly different trends. Most notably, the order of ligand binding to a given metal and the order of metal binding to a given ligand are the same on the three levels of theory. The energy difference between bidentate and monodentate binding to a given metal is also similar and thus remains small (Table 2). One obtains the same results for the energy balance ΔE_{react} (Table 4) of the isodesmic reaction (Figure 11) on all tested levels of theory; i.e., two monodentate ligands are always preferred, and this preference increases toward smaller cations. While we do not report the uncorrected values for interaction energies in this paper, it should also be noted that the BSSE correction carried out has a negligible influence on ΔE and especially the trends derived (Table S2).

Like in all modeling studies, another important issue concerns the search for "the global energy minimum", or, in a more modest perspective, to assess how reasonable are the model-built structures. Hunting for the absolute minimum is not an easy task,[61] especially when QM methods are used. For the present complexes, the conformational freedom is in fact quite restricted. We thus decided to test alternative starting structures. For the $EuCl_3\mathbf{L_{OO}}$ complex, two independent optimizations, respectively starting from the optimized cis $Eu\mathbf{L}^{3+}$ complex to which anions were added, or from an $EuCl_3$ (planar) salt to which **L** cis was added, were found to lead to identical arrangements. Other optimizations started from available X-ray structures retrieved from the Cambridge Database,[62] where NO_3^- were replaced by Cl^- anions, and water molecules (if any) were removed. Thus, optimization of the $EuCl_3\mathbf{L_{OO}}$ 1:1 complexes, which started from the $Yb(NO_3)_3(H_2O)$(dmpma) (refcode RIMQOT) as well from the $Nd(NO_3)_3(H_2O)_2$(dmpma) structures (refcode RIMQIN), also converged to the same energy and structure as the modelbuilt ones. For the 1:2 complexes, there is a priori more conformational freedom than for the 1:1 complexes. However, re-optimization of the $LaCl_3(\mathbf{L_{OO}})_2$ complex, starting from the $La(NO_3)_3$(tema) structure (refcode WEXMOB), and of the $EuCl_3(\mathbf{L_{OO}})_2$ complex, starting from the $Nd(NO_3)_3(tema)_2$ structure (refcode WATYOF) also lead to structures and energies that were identical to the model-built ones. We also note that upon minimization, large reorganization (like trans to cis conversion in $\mathbf{L}H^+$, or cis to trans rearrangement in $YbCl_3(\mathbf{L_{SS}})_2$) was sometimes observed, indicating that the minimizer is quite robust and that the optimized structures are not trapped in metastable states and should be at, or close to "absolute minima".

4. Conclusions

Quantum mechanical investigations reveal important aspects of the coordination of diamide ligands and their thia-analogues to lanthanide(III) cations in the gas phase. For the ligands **L** the metal binding gets stronger with increasing proton basicity, which means that the more basic oxygen binding sites are preferred over sulfur binding sites, and the M−**L** interaction strength decreases in the order $\mathbf{L_{OO}} > \mathbf{L_{OS}} > \mathbf{L_{SS}}$. For the metal cations M^{3+} the decisive intrinsic property is their size (or hardness), and the M−**L** interaction strength increases with decreasing size (growing hardness) in the $M\mathbf{L}^{3+}$ complexes, in the order $La^{3+} < Eu^{3+} < Yb^{3+}$. If the +3 cation charge is balanced by counterions ($MCl_3\mathbf{L}$ complexes) the studied ligands loose their cation discriminating features to a large extent. When a second ligand **L** is added ($MCl_3\mathbf{L}_2$ complexes) the effects of steric crowding in the first cation coordination shell become significant: the cation preferences of the different **L** shift toward larger cations, and in the case of $YbCl_3(\mathbf{L_{SS}})_2$ one even observes a change of the binding mode of one of the ligands from bidentate to monodentate. Steric crowding in the first coordination sphere of the metal is therefore of utmost importance in the search for suitable ligands for the liquid−liquid extraction of lanthanide and actinide cations, because it may critically influence the cation selectivity, and it is an important way to avoid unwanted coordination of solvent molecules. Steric crowding may be influenced by additional ligands (for instance "synergistic ligands" used in extraction experiments[63]) as well as by changing the size and nature of coordinated anions. It increases with the cation hardness (e.g., from La^{3+} to Yb^{3+} for a given ligand) as well as upon O → S substitution in the ligand.

Another important result is the small energy difference between monodentate and bidentate coordination of all studied ligands in $MCl_3\mathbf{L}$ complexes. While bidentate binding is preferred by $\mathbf{L_{OO}}$ and $\mathbf{L_{SS}}$ in the gas phase, $\mathbf{L_{OS}}$ even slightly prefers the monodentate binding mode via the oxygen binding site. The preference for bidentate coordination of $\mathbf{L_{OO}}$ and $\mathbf{L_{SS}}$ (less than 3 kcal/mol) is small enough to be easily compensated by additional ligands, by second shell hydrogen bond interactions with the free oxygen binding site (e.g., upon extraction of water or nitric acid[64]), and by substituent effects.[30,31,58] Thus, when the first coordination sphere of the metal is more saturated, monodentate binding might be enthalpically preferred by the symmetric $\mathbf{L_{OO}}$ and $\mathbf{L_{SS}}$ ligands as well. It should be noticed, however, that in solution freed space around the cation is taken by another ligand or solvent molecule, thus causing an entropy loss, which could increase the preference for bidentate coordination again. The experimental observation of dominant bidentate complexes in the solid state[23,26,29,30,32] as well as in solution[23] hints at the importance of entropy effects.

We did not explore the monodentate coordination of ligands in the more saturated $MCl_3\mathbf{L_2}$ complexes, where steric strain is larger than in $MCl_3\mathbf{L}$ complexes. Thus, the bidentate $MCl_3\mathbf{L_2}$ complexes remained so during the optimization. The only exception concerns the $YbCl_3(\mathbf{L_{SS}})_2$ complex, which spontaneously became monodentate, showing that the limit where steric strain induces a change from bidentate to monodentate binding mode has been reached, despite the relatively small coordination number.

The availability of a free, partially negative binding site in the monodentate malonamide complexes presumably enhances their ability to interact with polar solvents and thus lets them become more hydrophilic. This has to be kept in mind when evaluating their properties in liquid−liquid extraction. The small difference between the two coordination modes is also important for the design of ligands with multiple binding sites for lanthanide coordination. It would be of great interest to investigate the monodentate vs bidentate binding of cations by

malonamides grafted onto organized rigid platforms such as calixarene, in connection with the cation binding mode and related hydrophobicity and extractability of the formed complex.

Our calculations of a "chelate effect" isodesmic reaction with MCl_3**L** show that coordination of two monodentate amide ligands is markedly preferred over bidentate coordination of a diamide ligand. This points to the importance of intraligand strain in the competition of the monodentate and bidentate binding modes, as in the bidentate binding mode the O−C or S−C dipoles assume parallel positions and repulse each other. This strain increases with the cation charge and hardness, because these effects strengthen the O−C dipoles by polarization. It also increases from oxygen to sulfur binding sites, as well as with the size of the coordinated anions. In conformationally locked cis ligands or analogues, the prebuilt intraligand strain should lead to a marked stabilization of the bidentate form.

Finally, interligand steric crowding also affects the competition between the different binding modes. This is visible in the aforementioned binding mode change in $YbCl_3(\mathbf{L}_{SS})_2$, as well as in experimental studies. For example, in a 1:5 lanthanum complex of malonamide the ligands partially loose bidentate coordination to the metal.[32] In succinamide complexes with lanthanides, all ligands are bidentate when the counterions are perchlorates or triflates,[65] which themselves do not bind directly to the cation, whereas some can be monodentate, with respect to one cation, when directly bound nitrate counterions are used.[66] This binding mode change is presumably related to the enhanced steric crowding from the anions in the first coordination sphere. To summarize, the factors "steric crowding" and bidentate vs monodentate binding modes are strongly related,[8,34] and each have a large influence on the properties of diamides and related polyfunctional ligands in lanthanide and actinide chemistry.

Note Added in Proof

A recently published investigation on lanthanide complexes of CMPO also indicates a weak energy preference for bidentate vs monodentate binding modes: Boehme, C.; Wipff, G. *Inorg. Chem.* **2002**, *42*, 727−737.

Acknowledgment. We are grateful to CNRS IDRIS, CINES, and Université Louis Pasteur for computer resources and to the EEC (FIKW-CT-2000-0088 contract) and PRACTIS for support. G.W. thanks Prof. C. Madic for stimulating discussions.

Supporting Information Available: Tables of total energies of the calculated systems, interaction and relative energies, and coordinates of the complexes. This material is available free of charge via the Internet at http://pubs.acs.org.

References and Notes

(1) Alexander, V. *Chem. Rev.* **1995**, *95*, 273−342.

(2) Cecille, L.; Casarci, M.; Pietrelli, L. *New Separation Chemistry Techniques for Radioctive Waste and other Specific Applications*; Commission of the European Communities; Elsevier Applied Science: London, New York, 1991.

(3) Choppin, G. R.; Nash, K. L. *Radiochim. Acta* **1995**, *70/71*, 225−236.

(4) Choppin, G. R.; Peterman, D. R. *Coord. Chem. Rev.* **1998**, *174*, 283−299.

(5) Sabbatini, N.; Mecati, A.; Guardigli, M.; Balzani, V.; Lehn, J. M.; Ziessel, R.; Ungaro, R. *J. Luminescence* **1991**, *48−49*, 463−468.

(6) Horrocks, W. D. J.; Sudnik, D. R. *J. Am. Chem. Soc.* **1979**, *101*, 334−340.

(7) Parker, D.; Williams, J. A. G. *J. Chem. Soc., Dalton Trans.* **1996**, 3613−3628.

(8) Hancock, R. D.; Martell, A. E. *Chem. Rev.* **1989**, *89*, 1875−1914 and references therein.

(9) Comba, P. *Coord. Chem. Rev.* **1999**, *185−186*, 81−98.

(10) Boeyens, J. C. A.; Comba, P. *Coord. Chem. Rev.* **2001**, *212*, 3−10.

(11) Clement, O.; Rapko, B. M.; Hay, B. P. *Coord. Chem. Rev.* **1998**, *170*, 203−243.

(12) Reichert, D. E.; Welch, M. J. *Coord. Chem. Rev.* **2001**, *212*, 111−131.

(13) Hutschka, F.; Troxler, L.; Dedieu, A.; Wipff, G. *J. Phys. Chem. A* **1998**, *102*, 3773−3781.

(14) Troxler, L.; Dedieu, A.; Hutschka, F.; Wipff, G. *J. Mol. Struct. (THEOCHEM)* **1998**, *431*, 151−163.

(15) Schurhammer, R.; Erhart, V.; Troxler, L.; Wipff, G. *J. Chem. Soc., Perkin Trans. 2* **1999**, 2515−2534.

(16) Boehme, C.; Wipff, G. *J. Phys. Chem. A* **1999**, *103*, 6023−6029.

(17) Baaden, M.; Berny, F.; Boehme, C.; Muzet, N.; Schurhammer, R.; Wipff, G. *J. Alloys Compounds* **2000**, *303−304*, 104−111.

(18) Berny, F.; Muzet, N.; Troxler, L.; Dedieu, A.; Wipff, G. *Inorg. Chem.* **1999**, *38*, 1244−1252.

(19) Nigond, L.; Condamines, N.; Cordier, P. Y.; Livet, J.; Madic, C.; Cuillerdier, C.; Musikas, C. *Sep. Sci. Technol.* **1995**, *30*, 2075−2099.

(20) Musikas, S.; Vitorge, P.; Fitoussi, R.; Bonin, M.; Vialard-Goudou, D. P. International Symposium on Actinide Recovery. *Abstracts of Papers*; 182nd National Meeting of the American Chemical Society; American Chemical Society: Washington, DC, 1981, pp 1−14.

(21) Condamines, N.; Musikas, C. *Solv. Extract. Ion Exch.* **1992**, *10*, 69−100.

(22) Pathak, P. N.; Kumbhare, L. B.; Manchanda, V. K. *Sol. Extract. Ion Exch.* **2001**, *19*, 105−126.

(23) den Auwer, C.; Charbonnel, M. C.; Drew, M. G. B.; Grigoriev, M.; Hudson, M. J.; Iveson, P. B.; Madic, C.; Nierlich, M.; Presson, M. T.; Revel, R.; Russell, M. L.; Thuéry, P. *Inorg. Chem.* **2000**, *39*, 1487−1495.

(24) Arnaud-Neu, F.; Barboso, S.; Berny, F.; Casnati, A.; Muzet, N.; Pinalli, A.; Ungaro, R.; Schwing-Weil, M. J.; Wipff, G. *J. Chem. Soc., Perkin Trans. 2* **1999**, 1727−1738.

(25) McKervey, A.; Schwing, M.-J.; Arnaud-Neu, F. In *Comprehensive Supramolecular Chemistry*; Atwood, J. L., Davies, J. E. D., McNicol, D. D., Vögtle, F., Lehn, J.-M., Eds.; Pergamon: New York, 1996; pp 537−603.

(26) Castellano, E. E.; Becker, R. W. *Acta Crystallogr. B* **1981**, *37*, 61−67.

(27) Thuéry, P.; Nierlich, M.; Charbonnel, M.-C.; Dognon, J.-P. *Acta Crystallogr. C* **1999**, *C55*, 1434−1435.

(28) Thuéry, P.; Nierlich, M.; Charbonnel, M.-C.; den Auwer, C.; Dognon, J.-P. *Polyhedron* **1999**, *18*, 3599−3603.

(29) Byers, P.; Drew, M. G. B.; Hudson, M. J.; Isaacs, N. S.; Madic, C. *Polyhedron* **1994**, *13*, 349.

(30) Chan, G. Y. S.; Drew, M. G. B.; Hudson, M. J.; Iveson, P. B.; Liljenzin, J.-O.; Skalberg, M.; Spjuth, L.; Madic, C. *J. Chem. Soc., Dalton Trans.* **1997**, 649−660.

(31) Iveson, P. B.; Drew, M. G. V.; Hudson, M. J.; Madic, C. *J. Chem. Soc., Dalton Trans.* **1999**, 3605−3610.

(32) Castellano, E. E.; Becker, R. W. *Acta Crystallogr. Sect. B* **1981**, *37*, 1998.

(33) Martell, A. E.; Hancock, R. D. *Metal Complexes in Aqueous Solutions*; Plenum Press: New York, 1996.

(34) Martell, A. E.; Hancock, R. D.; Motekaitis, R. J. *Coord. Chem. Rev.* **1994**, *133*, 39−65 and references therein.

(35) Lehn, J. M. *Struct. Bonding* **1973**, *161*, 1−69.

(36) Chen, J.; Zhu, Y.; Jiao, R. *Sep. Sci. Technol.* **1996**, *31*, 2724−2731.

(37) Hill, C.; Madic, C.; Baron, P.; Ozawa, M.; Tanaka, Y. *J. Alloys Compounds* **1998**, *271−273*, 159−162.

(38) Pearson, R. G. *Hard and Soft Acids and Bases*; Dowdon, Hutchinson and Ross: Stroudsburg, PA, 1973.

(39) Choppin, G. R. In *Principles of Solvent Extraction*; Rydberg, J,. Musikas, C., Choppin, G. R., Eds.; M. Dekker, New York, 1992; pp 71−100.

(40) Frisch, M. J.; Trucks, G. W.; Schlegel, H. B.; Scuseria, G. E.; Robb, M. A.; Cheeseman, J. R.; Zakrzewski, V. G.; Montgomery, J. A., Jr.; Stratmann, R. E.; Burant, J. C.; Dapprich, S.; Millam, J. M.; Daniels, A. D.; Kudin, K. N.; Strain, M. C.; Farkas, O.; Tomasi, J.; Barone, V.; Cossi, M.; Cammi, R.; Mennucci, B.; Pomelli, C.; Adamo, C.; Clifford, S.; Ochterski, J.; Petersson, G. A.; Ayala, P. Y.; Cui, Q.; Morokuma, K.; Malick, D. K.; Rabuck, A. D.; Raghavachari, K.; Foresman, J. B.; Cioslowski, J.; Ortiz, J. V.; Stefanov, B. B.; Liu, G.; Liashenko, A.; Piskorz, P.; Komaromi, I.; Gomperts, R.; Martin, R. L.; Fox, D. J.; Keith, T.; Al-Laham, M. A.; Peng, C. Y.; Nanayakkara, A.; Gonzalez, C.; Challacombe, M.; Gill, P. M. W.; Johnson, B. G.; Chen, W.; Wong, M. W.; Andres, J. L.; Head-Gordon, M.; Replogle, E. S.; Pople, J. A. *Gaussian 98*, revision A.5; Gaussian, Inc.: Pittsburgh, PA, 1998.

(41) Boys, S. F.; Bernardi, F. *Mol. Phys.* **1970**, *19*, 553−566.

(42) Maron, L.; Eisenstein, O. *J. Phys. Chem. A* **2000**, *104*, 7140−7143.

(43) Hong, G.; Schautz, F.; Dolg, M. *J. Am. Chem. Soc.* **1999**, *121*, 1, 1502−1512.

(44) Dolg, M.; Stoll, H.; Preuss, H. *J. Chem. Phys.* **1989**, *90*, 1730−1734.

(45) Dolg, M.; Stoll, H.; Savin, A.; Preuss, H. *Theor. Chim. Acta* **1993**, *85*, 441.

(46) Ehlers, A. W.; Böhme, M.; Dapprich, S.; Gobbi, A.; Höllwarth, A.; Jonas, V.; Köhler, K. F.; Stegmann, R.; Veldkamp, A.; Frenking, G. *Chem. Phys. Lett.* **1993**, *208*, 111.

(47) Dunning, T. H.; Hay, P. J. In *Methods of electronic structure theory. Modern Theoretical Chemistry 3*; Schaefer, H. F., III, Ed.; Plenum Press: New York, 1977; pp 1−28.

(48) Sandrone, G.; Dixon, D. A.; Hay, B. P. *J. Phys. Chem.* **1999**, *103*, 3, 3554−3561.

(49) Berny, F.; Wipff, G. *J. Chem. Soc., Perkin Trans. 2* **2001**, 73−82.

(50) Kebarle, P. *Annu. Rev. Phys. Chem.* **1977**, *28*, 445−476.

(51) This change in binding mode is found without any a priori assumption on the nature of the metal−ligand M−**L** bond, or on "steric effects". This contrasts with force field approaches based on a priori description of the M−**L** bond and of "steric effects". Most force fields that use covalent representations of M−**L** bonds (e.g., MM3 derived; see, for example, refs 9, 12, and 34) do not allow for changes in coordination number upon minimization and estimate the "strain" (van der Waals term only, without electrostatic component) as a function of the coordination number. Alternative approaches, based on noncovalent representations of the M···**L** interactions, allow in principle for changes in ligand binding mode upon minimization but require a careful calibration of electrostatic effects (including charge transfer, polarization, and many body interactions) and deeply related steric effects. It is also important to point out that that the metal coordination number may be different (generally lower) in the gas phase, compared to condensed phases. For instance, for the $Na(H_2O)_6^+$ aggregate, the most stable arrangement in the gas phase is 4+2 (4 water molecules in the first shell + 2 in the second shell) rather than 6+0,[52,53] while in aqueous solution, the CN of Na^+ is close to 6.0.[54] Similar effects have been reported for La^{3+} hydrates.[55] Thus, care must be taken in the interpretation of "steric effects" and coordination numbers in condensed phase in terms of metal−ligand and ligand−ligand interactions only.

(52) Kim, J.; Lee, S.; Cho, S. J.; Mhin, B. J.; Kim, K. S. *J. Chem. Phys.* **1995**, *102*, 839−849.

(53) Feller, D.; Glendening, E. D.; Woon, D. E.; Feyereisen, M. W. *J. Chem. Phys.* **1995**, *103*, 3526−3542.

(54) Marcus, Y. *Ion Solvation.*; Wiley: Chichester, U.K., 1985.

(55) Derepas, A.-L.; Soudan, J.-M.; Brenner, V.; Dognon, J.-P.; Millié, P. *J. Comput. Chem.* **2002**, *23*, 1013. G.W. thanks the authors for providing a preprint of this paper.

(56) Schwarzenbach, G. *Helv. Chim. Acta* **1952**, *35*, 2344.

(57) Hancock, R. D. *Prog. Inorg. Chem.* **1989**, *37*, 187−291. According to QM calculations on lanthanide complexes with bifunctional carbonyl or phosphoryl bidentate ligands, formation of a seven-chelate ring with the metal is intrinsically preferred over the six-chelate ring in the gas phase (B. Coupez, G. Wipff, unpublished.)

(58) Spjuth, L.; Liljenzin, J. O.; Hudson, M. J.; Drew, M. G. B.; Iveson, P. B.; Madic, C. *Solv. Extr. Ion Exch.* **2000**, *18*, 1−23.

(59) Boehme, C.; Wipff, G. *Inorg. Chem.* **1999**, *38*, 5734−5741.

(60) Spencer, S.; Gagliardi, K.; Handy, N. C.; Ioannou, A. G.; Skylaris, C.-K.; Willetts, A.; Simper, A. M. *J. Phys. Chem. A* **1999**, *103*, 1831−1837.

(61) Saunders: M.; Houk, K. N.; Wu, Y. D.; Still, W. C.; Lipton, M.; Chang, G.; Guida, W. C. *J. Am. Chem. Soc.* **1990**, *112*, 1419−1427.

(62) Allen, F. H.; Kennard, O. *Chemical Design Automation News* **1993**, *8*, 31−37.

(63) Ionova, G.; Ionov, S.; Rabbe, C.; Hill, C.; Madic, C.; Guillaumont, R.; Krupa, J. C. *Solv. Extract. Ion Exch.* **2001**, *19*, 391−414.

(64) Nigond, L.; Musikas, C.; Cuillerdier, C. *Solv. Extract. Ion Exch.* **1995**, *12*, 261−297.

(65) Rapko, B. M.; McNamara, B. K.; Rogers, R. D.; Broker, G. A.; Lumetta, G. J.; Hay, B. P. *Inorg. Chem.* **2000**, *39*, 4858−4867.

(66) Rapko, B. M.; McNamara, B. K.; Rogers, R. D.; Lumetta, G. J.; Hay, B. P. *Inorg. Chem.* **1999**, *38*, 4585−4592.